Structure of the histidine-containing phospho-transfer (HPt) domain of the anaerobic sensor protein ArcB complexed with the chemotaxis response regulator CheY

Masato Kato,[a] **Toshiyuki Shimizu,**[a] **Takeshi Mizuno**[b] **and Toshio Hakoshima**[a]*

[a]Department of Molecular Biology, Nara Institute of Science and Technology, 8916-5 Takayama Ikoma, Nara 630-0101, Japan, and [b]School of Agricultural Science, Nagoya University, Chikusaku, Nagoya 464-01, Japan

Correspondence e-mail:
hakosima@bs.aist-nara.ac.jp

The three-dimensional structure of the HPt domain of ArcB complexed with CheY has been determined using the molecular-replacement method. The structure was refined to a crystallographic R factor of 18.3% at 2.68 Å resolution. The final model included 1899 protein atoms (117 residues from the HPt domain and 128 residues from CheY), one sulfate ion and 44 solvent molecules. In the crystal, CheY molecules stacked along the a axis of the cell with no interactions between neighbouring rows and the HPt domain bridged the CheY molecules. The phosphodonor residue His715 was fully exposed to the solvent region, even though the HPt domain was in contact with four molecules of CheY. CheY showed significant conformational change. This indicates that the HPt domain has a rigid structure when complexed with CheY.

1. Introduction

The *Escherichia coli* sensor kinase ArcB is responsive to anaerobic conditions: it phosphorylates the response regulator ArcA. The phosphorylated ArcA directly or indirectly regulates some 30 operons which adapt the respiratory system of the cell to anaerobic conditions (Iuchi *et al.*, 1990; Lynch & Lin, 1996). ArcB has four domains: a receptor domain, an HPK domain, a receiver domain and a histidine-containing phosphotransfer (HPt) domain. The HPt domain contains the conserved histidine residue, which can be phosphorylated. A phosphoryl group is thought to be transferred in the sequence HPK domain, receiver domain, HPt domain, receiver domain of ArcA (Ishige *et al.*, 1994; Tsuzuki *et al.*, 1995; Georgellis *et al.*, 1997).

We focused our attention on the structure and function of the HPt domain of ArcB. Using 2.06 Å resolution data (Kato *et al.*, 1997), we determined the structure of the HPt domain to be an all-α structure with six helices, including a four-helix bundle motif. We also found that the structure of the HPt domain was similar to the NMR structure of the N-terminal P1 domain of the chemotaxis sensor kinase CheA of *E. coli*. In addition, we also showed that the HPt domain of ArcB phosphorylates the non-recognizable response regulator CheY, which is the recognizable response regulator for CheA (Yaku *et al.*, 1997). These results suggested that ArcB might be a dual signal transmitter and that CheY might be another target receiver for ArcB. The possible biological significance of this hypothesis is that anaerobic stimuli act as repellent signals and cells try to escape from anaerobic conditions by tumbling their flagella. All receiver domains identified to date are believed to fold into the same $(\alpha/\beta)_5$ fold as CheY (Baikalov *et al.*, 1996; Madhusudan *et al.*, 1996; Volkman *et al.*, 1995; Djordjevic *et al.*, 1998). There is as yet little experimental evidence to define the determinants of specificity necessary to

Table 1
Data-collection statistics.

Values in parentheses refer to the outer shell (2.82–2.68 Å).

Resolution (Å)	2.68
Measured reflections	40201
Unique reflections	9407
Completeness (%)	91.7 (75.8)
R_{merge}† (%)	7.2 (40.5)

† $R_{merge} = \sum_{hkl}\sum_{i}|I_i(hkl) - \langle I(hkl)\rangle| / \sum_{hkl}\sum_i I_i(hkl)$, where $\langle I \rangle$ is the average intensity of the i observations of reflection hkl.

Table 2
Refinement statistics.

Resolution range (Å)	10.0–2.68
Number of reflections used	
Total $[F \geq \sigma(F)]$	9146 (90.6% completeness)
Working set	8658
Test set (5% of total)	488
R factor† (%)	18.3
Outer shell (2.80–2.68 Å) (%)	31.2
Free R factor† (%)	25.0
Number of residues‡	HPt 117, CheY 128
Number of protein atoms	1899
Number of sulfate ions	1
Number of solvent molecules	44
Mean B factor (Å²)	41.0
R.m.s. deviations	
Bonds (Å)	0.007
Angles (°)	1.3
Dihedrals (°)	21
Impropers (°)	1.2

† R factor (or free R factor) $= \sum_{hkl}||F_{obs}(hkl)| - |F_{calc}(hkl)|| / \sum_{hkl}|F_{obs}(hkl)|$, where $F_{obs}(hkl)$ is the observed structure factor and $F_{calc}(hkl)$ is the calculated structure factor from the refined model. ‡ Missing residues: six residues at the N-terminus and two residues at the C-terminus of the HPt domain.

identify the appropriate receiver domain in any system. To clarify the molecular recognition of these response regulators by the HPt domain at an atomic level, we determined the crystal structure of the ArcB HPt domain complexed with CheY.

2. Materials and methods

2.1. Preparation of proteins

E. coli K-12 strain DZ225 carrying plasmid pSU2DH encoding the HPt domain has been constructed previously (Nagasawa *et al.*, 1992; Ishige *et al.*, 1994). Construction of *E. coli* strain BL21 carrying plasmid pT7-CheY has also been described previously (Yaku *et al.*, 1997). Overexpression and purification of the HPt domain and CheY were carried out according to a method described previously (Kato *et al.*, 1996, 1998). The purified HPt domain and CheY were concentrated to 75 and 63 mg ml⁻¹, respectively, using Centricon-10 (Amicon, USA). They were mixed together and then diluted to a concentration of 25.5 mg ml⁻¹ using stock buffer (5 m*M* Bis–Tris pH 7.0, 100 m*M* NaCl). This solution was stored at 277 K. Protein purity was confirmed by 17.5% SDS–poly-acrylamide gel electrophoresis, staining with Coomassie Blue G-250.

Table 3
Results of the molecular replacement with *AMoRe*.

For comparison, the top two solutions are listed in each step.

Rotation-function search of the HPt domain – *AMoRe*.

α	β	γ	x	y	z	CC†	R‡
66.49	65.95	347.88	0.000	0.000	0.000	11.4	0.0
120.34	74.33	105.18	0.000	0.000	0.000	9.6	0.0

Rotation-function search of the HPt domain – *X-PLOR*§.

α¶	β¶	γ¶	No.††	PC1‡‡	PC2‡‡
68.61	68.33	346.92	1	0.0709	0.0779
32.49	86.77	343.43	14	0.0465	0.0521

Translation-function search of the HPt domain.

α	β	γ	x	y	z	CC†	R‡
66.49	65.95	347.88	0.4897	0.9956	0.1197	36.7	49.6
117.83	65.64	325.51	0.1242	0.1144	0.1729	30.0	51.3

Rigid-body refinement of the HPt domain.

α	β	γ	x	y	z	CC†	R‡
68.27	67.92	347.28	0.4926	0.9951	0.1236	41.8	48.0
111.14	46.57	22.09	0.3899	0.1803	0.4503	32.4	51.4

Translation-function search of CheY, fixing the HPt domain.

α	β	γ	x	y	z	CC†	R‡	
68.27	67.92	347.28	0.4926	0.9951	0.1236			HPt
60.83	74.50	144.54	0.5065	0.6547	0.9912	57.3	41.8	CheY1
100.23	71.32	230.26	0.1615	0.7496	0.5600	38.1	48.9	CheY2

Rigid-body refinement of CheY and the HPt domain.

α	β	γ	x	y	z	CC†	R‡	
59.15	74.13	143.80	0.5037	0.6544	0.6893	61.0	40.3	CheY1
69.91	68.13	346.90	0.4937	0.9946	0.1231	61.0	40.3	HPt
108.50	73.57	36.27	0.8178	0.3049	0.4929	40.7	48.8	CheY2
68.23	67.98	347.48	0.4905	0.9955	0.1214	40.7	48.8	HPt

† Correlation coefficient. ‡ R factor. § These values were the results after PC-refinement. ¶ The rotation function θ_1, θ_2 and θ_3 were converted by *CONVROT* (Urzhumtseva & Urzhumtsev, 1997). †† The order of peaks before PC-refinement (Brünger, 1990). ‡‡ The PC value before and after PC-refinement.

2.2. Crystallization and data collection

The crystals of the HPt–CheY complex were obtained under the conditions described previously (Kato *et al.*, 1998). The crystals belonged to the orthorhombic system, space group $P2_12_12_1$, with unit-cell parameters $a = 55.18$, $b = 76.17$, $c = 83.27$ Å. X-ray diffraction data were collected at the BL-18B beamline station at the Photon Factory, Tsukuba (Kato *et al.*, 1998). Data processing was performed using the program *WEIS* (Higashi, 1989). Data-processing statistics are given in Table 1.
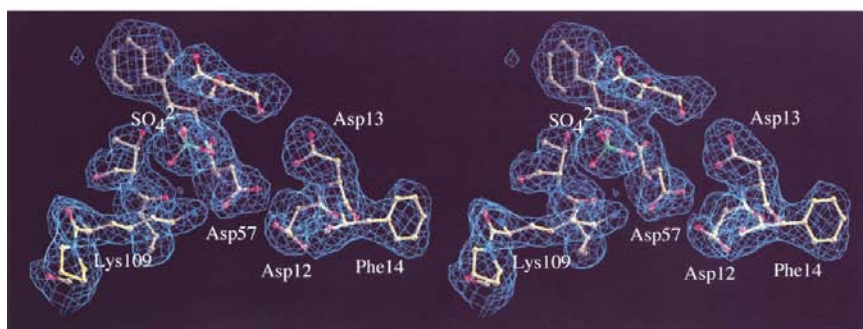
2.3. Structure solution and refinement

The synchrotron data set was used to solve the structure by the molecular-replacement method using the programs *AMoRe* (Navaza, 1994) and *X-PLOR* (Brünger, 1992). Data
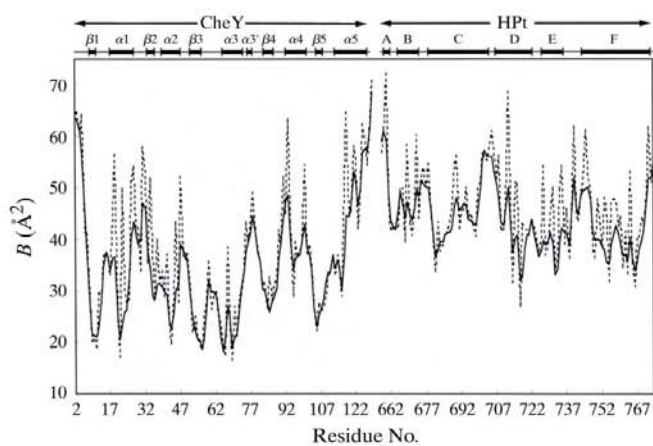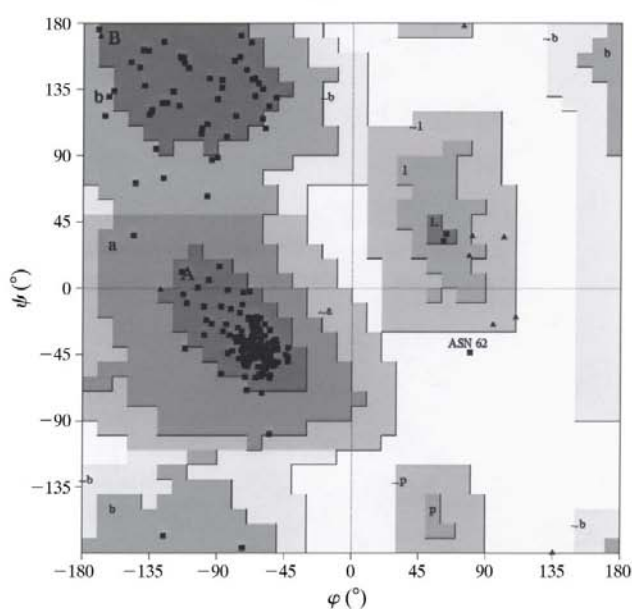
Figure 1
(*a*) The average *B* factors for the main-chain (unbroken lines) and side-chain atoms (dashed lines) of each residue are plotted as a function of the residue number with the schematic secondary structure. (*b*) Ramachandran plot. Glycine residues are denoted by triangles and all other residues by squares. One labelled residue in the disallowed region is Asn62 of CheY. The different regions defined by borderlines are labelled: A, B, L, most favoured; a, b, l, p, allowed and ~a, ~b, ~l, ~p, generously allowed. (*c*) An example of the quality of the electron-density maps. The active site of CheY is shown as a $2F_o - F_c$ map calculated using data in the 10.0–2.68 Å resolution range. Contours are at the 1.0σ level. Four residues, Asp12, Asp13, Asp57 and Lys109, which are highly conserved in the CheY superfamily, are labelled along with Phe14 and a sulfate ion.

were used in the resolution range 8.0–3.0 Å. Conversion of the *X-PLOR* rotation functions to those of *AMoRe* was achieved using the program *CONVROT* (Urzhumtseva & Urzhumtsev, 1997). The models were repositioned using the program *PDBSET* (Collaborative Computational Project, Number 4, 1994) with the final solutions of the molecular replacement. The initial electron-density map was improved using the program *DM* (Cowtan & Main, 1996) with solvent flattening and histogram matching. Model building was accomplished using the graphics program *O* (Jones *et al.*, 1991).

Refinement was carried out using the program *X-PLOR* with bulk-solvent correction of the structure factors. In refinement cycles using the simulated-annealing method with data in the 10–3 Å resolution range, the *R* factor and free *R* factor (for 5% of all reflections) fell rapidly while maintaining reasonable stereochemistry. The resolution was then extended to 2.68 Å and refinement was continued. In the final round of refinement, water molecules were picked out from $F_o - F_c$ and $2F_o - F_c$ maps. One sulfate ion and 44 water molecules were assigned based on density in the maps, hydrogen-bonding potential and refined temperature factors of less than 65 Å^2 at full occupancy. Six N-terminal residues and two C-terminal residues of the HPt domain were disordered. Refinement statistics are given in Table 2.

A Ramachandran plot was produced using *PROCHECK* (Laskowski *et al.*, 1993). The secondary structure was assigned using *PROMOTIF* (Hutchinson & Thornton, 1996). Model figures were drawn with *MOLSCRIPT* (Kraulis, 1991) or *QUANTA* (Molecular Simulations Inc., USA). Since the numbering of the residues of the HPt domain was based on the recent correction to the SWISS-PROT file (code P22763), the residue number of the active histidine of the HPt domain is 715.

3. Results and discussion

3.1. Molecular replacement

The starting models were the HPt domain solved at 2.06 Å resolution (Kato *et al.*, 1997) and CheY which is not bound to an Mg^{2+} ion (apo-CheY) solved at 1.7 Å (Volz & Matsumura, 1991). Both the fast rotation-

function search in *AMoRe* and the direct rotation-function search in *X-PLOR* were carried out for each model. The top HPt domain peaks from *AMoRe* and *X-PLOR* corresponded to the same orientation of the rotation function (Table 3). Translation searches and rigid-body refinement with *AMoRe* emphasized the contrast in the correlation coefficients and *R* values. In the molecular replacement of CheY, similar results were obtained (data not shown). Because of the possibility that the origins of these solutions had nothing in common, the translation searches for the orientations of CheY were carried out by fixing the top solution of the HPt domain, followed by rigid-body refinement. The first set gave an *R* factor of 40.3%, which was clearly distinguishable from other solutions. The translation searches for the orientations of the HPt domain were also carried out by fixing the top solution of CheY and gave an equivalent solution (data not shown). The models repositioned by the functions of these solutions showed excellent crystal packing. The electron-density map calculated after the density modification was clear and it was easy to rebuild the models.

3.2. Quality of the models

The model of the HPt domain complexed with CheY comprised the 117 residues Lys658–Thr774 of ArcB and that of CheY complexed with the HPt domain comprised the 128 residues Ala2–Met129. The eight residues at the N- and C-termini of the HPt domain were invisible on the final $2F_o - F_c$ map, suggesting that they were disordered in the crystal. They were also disordered in the crystal of the HPt domain solved at 2.06 Å resolution (Kato *et al.*, 1997). Since the N-terminal methionine of CheY was cleaved post-translationally in the cell (Volz & Matsumura, 1991), the polypeptide chain used in this study started at residue Ala2. Fig. 1(*a*) shows the temperature factors for the main-chain and side-chain atoms plotted as a function of residue number. The averaged temperature factor for the atoms of the HPt domain
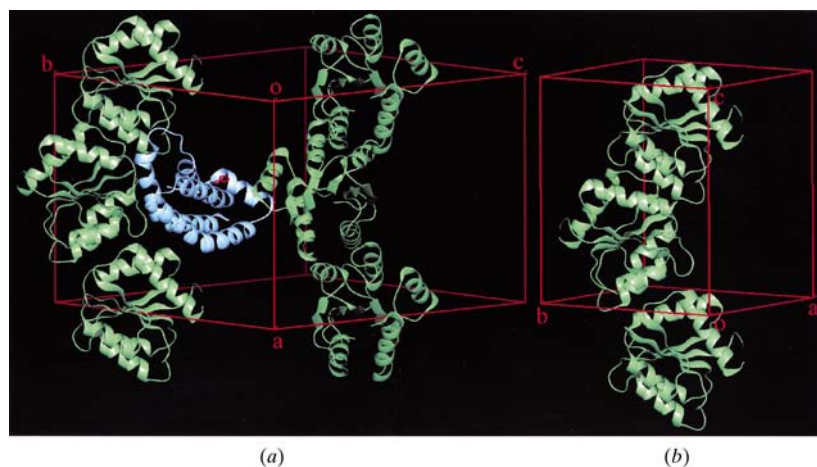
Table 4
Areas of and hydrogen bonds in the contact regions.

Region	Contact area (Å^2)	Hydrogen bond CheY	HPt	Distance (Å)
#1	465	Ala74 O	Trp751 NE1	2.8
		Glu100 O	Asp746 OD1	3.0
#2	537	Phe14 O	Glu754 OE2	3.8†
		Arg19 NH1	Glu750 OE1	3.8†
		Glu37 OE1	Glu757 OE1	3.2
		Glu37 OE2	Glu753 OE2	3.5†
		Asp38 OD1	Glu757 OE1	3.8†
#3	315	Glu27 OE2	Glu764 OE1	3.6†
		Glu27 OE2	His761 ND1	3.4
		Glu117 OE2	Arg760 NE	3.3
#4	742	Lys92 NZ	Gly722 O	3.4
		Tyr106 N	Leu674 O	4.0†
		Lys119 NZ	Val675 O	3.8†

† These are longer than the standard hydrogen bond.

was 45.8 Å^2 and that for the atoms of CheY was 36.6 Å^2. These higher temperature factors indicated that the molecules of the HPt domain and CheY were loosely packed owing to the weak interaction among them and the high solvent content (V_{solv} is 60%) of the crystal. The side-chain density of 12 hydrophilic residues (Glu660, Lys678, Lys689, Lys708, Glu712, Lys716, Glu745 and Lys772 of the HPt domain; Lys4, Lys26, Glu118, and Lys128 of CheY) were ambiguous, suggesting general disorder. A Ramachandran plot of the main-chain torsion angles (Ramachandran & Sasisekharan, 1968) showed that 194 non-glycine and non-proline residues (91.1%) fell into the most favoured regions and 18 residues (8.5%) were in the additional allowed regions (Fig. 1*b*). Only one non-glycine residue, Asn62 of CheY, was in a disallowed region. This residue was involved in a classical γ-turn which is conserved in CheY structures (Volz & Matsumura, 1991; Stock *et al.*, 1989, 1993; Bellsolell *et al.*, 1994). One solvent site, which was located in the active pocket of CheY, was originally modelled as a water molecule until it became apparent in the latter stages of refinement that its low temperature factors, large nonspherical electron-density envelopes and special ionic environments indicated it to be an SO_4^{2-} ion. It appears that no other ions added in the crystallization are present. The final *R* factor and free *R* factor of this model were 18.3 and 25.0%, respectively, for all data with $F \geq \sigma(F)$ in the 10–2.68 Å resolution range. The mean coordinate error for all atoms was estimated to be 0.30 Å, according to the method of Luzzati (1952). A representative region of the final electron-density map is given in Fig. 1(*c*).

3.3. Crystal packing and contact regions

The crystal packing of the HPt–CheY complex is shown in Fig. 2. This crystal contained one 1:1 complex in the asymmetric unit. From a global view, the CheY molecules arranged themselves into rows parallel to the *a* axis (55.2 Å) of the cell. Similar packing is shown in the crystal of apo-CheY (Volz & Matsumura,
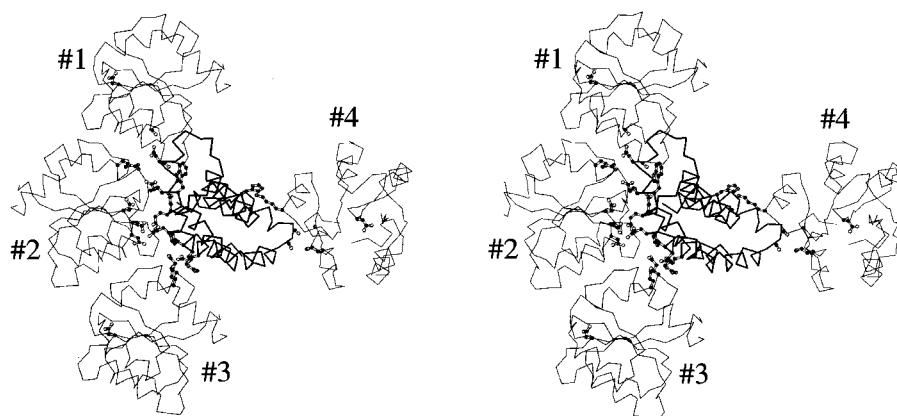

Figure 2
Crystal packing of the HPt–CheY complex and apo-CheY. (*a*) The crystal of the HPt–CheY complex contained one 1:1 complex in the asymmetric unit. Two rows of CheY molecules (green) are bridged by the HPt domain (blue). The active residue, His715, is drawn as a red stick model. (*b*) The same packing in the apo-CheY crystal (Volz & Matsumura, 1991). Cells are represented by red lines with labelled axes.

Figure 3
Stereo diagram showing the interactions between the HPt domain and CheY. The HPt domain is shown in thin lines and CheY in thick lines. The numbers labelled in the CheY molecules correspond to the contact regions. All residues involved in the contacts are shown as ball-and-stick models, with the active residues of the HPt domain and CheY being His715 and Asp57, respectively.
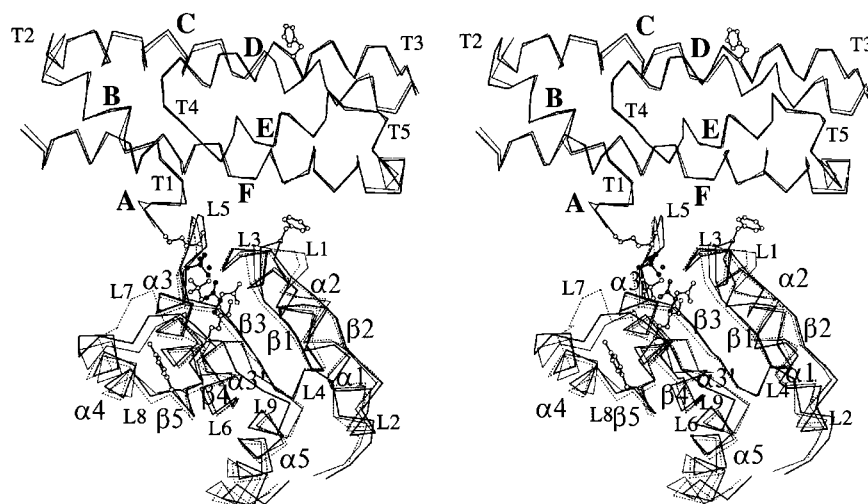

Figure 4
Stereo diagram showing the superposition of C_α traces of the HPt–CheY complex, the 2.06 Å HPt domain, apo-CheY and Mg^{2+}-CheY. The complex including contact region #2 is shown. The HPt domain and CheY in the complex are shown as thin lines, the 2.06 Å HPt domain and apo-CheY as thick lines and Mg^{2+}-CheY as dashed lines. The white ball-and-stick models are the residues Lys658, His715, Phe14, Asp57, Tyr106 and Lys109 and the SO_4^{2-} ion in the complex. The grey ball-and-stick models are the residue Asp57 and the Mg^{2+} ion in Mg^{2+}-CheY. The black ball-and-stick model is the SO_4^{2-} ion in apo-CheY.

1991). The rows of apo-CheY molecules are parallel to the *c* axis (54.0 Å). In other CheY crystals, which have similar unit-cell parameters and belong to the same space group, $P2_12_12_1$, similar packing exists and the axis parallel to the rows is roughly 54 Å long (Stock *et al.*, 1989, 1993; Zhu *et al.*, 1997). Furthermore, similar packing exists in the complex crystal between CheY and the P2 domain of CheA (McEvoy *et al.*, 1998). In this complex crystal, the rows of CheY molecules are parallel to the *b* axis, which is 64.2 Å long. The increase in unit-cell dimension may be a consequence of a decrease in interaction between the CheY molecules. The contact area between adjacent CheY molecules complexed with the P2 domains was 515 Å^2 and that between adjacent CheY molecules complexed with the HPt domains was 768 Å^2. The apo-

CheY molecules interacted with adjacent apo-CheY molecules in other rows, although no rows interacted with any other rows in the HPt–CheY complex crystal. Instead, the HPt domains formed bridges between the parallel rows of CheY molecules. The HPt domain made contacts with three CheY molecules in one row and with one molecule in the other row. The accessible area of each of the four contact regions, designated #1, #2, #3, and #4, was relatively small (each was <750 Å^2). Most of these contacts were formed mainly by weak hydrogen bonds or ion pairs (Fig. 3, Table 4).

3.4. Overall structure

A schematic drawing of the HPt–CheY complex structure, containing contact region #2, is shown in Fig. 4. The HPt domain has a kidney-shaped all-α structure which includes six helices (A–F). Helices D and E and halves of helices C and F form a four-helix bundle which is arranged in an up-and-down topology with a left-handed twist (Kato *et al.*, 1997). Although the HPt domain interacts with CheY in four regions, the folding of the HPt domain was in agreement with that of the 2.06 Å structure. The r.m.s. deviation of C_α positions between the two structures was 0.53 Å. Furthermore, the hydrogen bond between the active residue His715 and Gln737 remained. The substitution of Gln737 by an alanine decreased the activity of phosphotransfer owing to the loss of this hydrogen bond (unpublished data). These results confirmed the rigidity of the folding of the HPt domain.

CheY is a small single-domain protein consisting of a five-stranded parallel β-sheet core which is flanked by five α-helices (Volz, 1993). This structural feature is also conserved in the current structure, although the main-chain torsion angles of the residues 76–78 between $\alpha3$ and $\beta4$, which form a type I β-turn in other CheY structures, changed to form a 3_{10}-helix. Furthermore, significant differences occurred in the three loops (L1, L7, and L9) around the active pocket, which includes four functionally important residues, Asp12, Asp13, Asp57 and Lys109 (see below).

3.5. Comparison of structures

There were small differences between the current HPt domain complexed with CheY and the 2.06 Å HPt domain. Three regions of polypeptide chains showed differences with deviations greater than 1.0 Å (Fig. 5a). The N-terminal Lys658

was involved in contact region #2, and the NZ atom of the side chain participated in hydrogen bonding with a water molecule which was located between the HPt domain and CheY. It caused a change in the torsion angle ψ from 145 to $-21°$, resulting in a 2.0 Å movement of C_α. Another region containing differences was Glu673–Val675, which is located in the C-terminus of helix *B* and loop T2. These residues were involved in contact region #4. The weak hydrogen bond between Val675 of the HPt domain and Lys119 of CheY caused a shift of this region by a maximum of 1.4 Å and a shift of the starting residue of helix *C* by one residue from Pro677 to Lys678. Ala743 in loop T5, which was involved in contact region #1, was also repositioned by 1.6 Å away from CheY. The torsion angles (φ, ψ) of Pro742 changed from ($-59, -35°$) to ($-60, 135°$) and those of Ala743 from ($-93, 12°$) to ($61, 32°$) owing to the flipping of the peptide bond between them. On the Ramachandran plot, these changes indicated that the conformation of Pro742 changed from α-form to β-form and that of Ala743 from β-form to α_L-form. These large changes were induced in order to avoid steric clashes with CheY.

The structure of CheY resembled the apo-CheY structure (Volz & Matsumura, 1991) rather than the Mg^{2+}-CheY structure (Bellsolell *et al.*, 1994; Figs. 4 and 5*b*). The r.m.s. deviation in C_α positions was 1.1 Å between the current CheY and apo-CheY, whereas the difference was 1.7 Å when compared with Mg^{2+}-CheY. Among these three structures, there were three regions which showed significant differences with deviations greater than 2.0 Å.

The first region was loop L1, which is almost identical in apo-CheY and Mg^{2+}-CheY, and differs only in the current CheY. Loop L1 was involved in contact region #2 and interacted with helix *F* of the HPt domain. The main-chain O atom of Phe14 formed a weak hydrogen bond with the side-chain carboxyl O atom of Glu754 of the HPt domain. The conformational changes of residues Asp13–Ser15 caused the starting residue of the helix $\alpha1$ to shift back by one residue. In apo- and Mg^{2+}-CheY, Ser15 is the first residue of the helix, but Thr16 was the first helix residue in the current CheY. Phe14 was flipped out and the side chain moved far away from the active site. The aromatic ring of Phe14 in apo- and Mg^{2+}-CheY appeared to shield the active pocket. When Asp57 of CheY is phosphorylated by the phosphohistidine 715 of the HPt domain, this ring would have to rearrange in order to avoid steric collisions with the histidine. This open form of Phe14 was also seen in the complex structure between CheY and the P2 domain and causes a twofold increase in the solvent accessibility of Asp57 (McEvoy *et al.*, 1998).

The second region was loop L7, whose conformation has been shown to be changed on binding Mg^{2+} to the active pocket (Bellsolell *et al.*, 1994). The difference in this loop between the current CheY and Mg^{2+}-CheY was as large as that between apo-CheY and Mg^{2+}-CheY. Apo-CheY has an SO_4^{2-} ion in the active pocket (Volz & Matsumura, 1991). This supports our assignment of the excess electron density in the active pocket of CheY–HPt as an SO_4^{2-} ion. As a result of the rearrangement of loop L7, strand $\beta4$ elongated to the
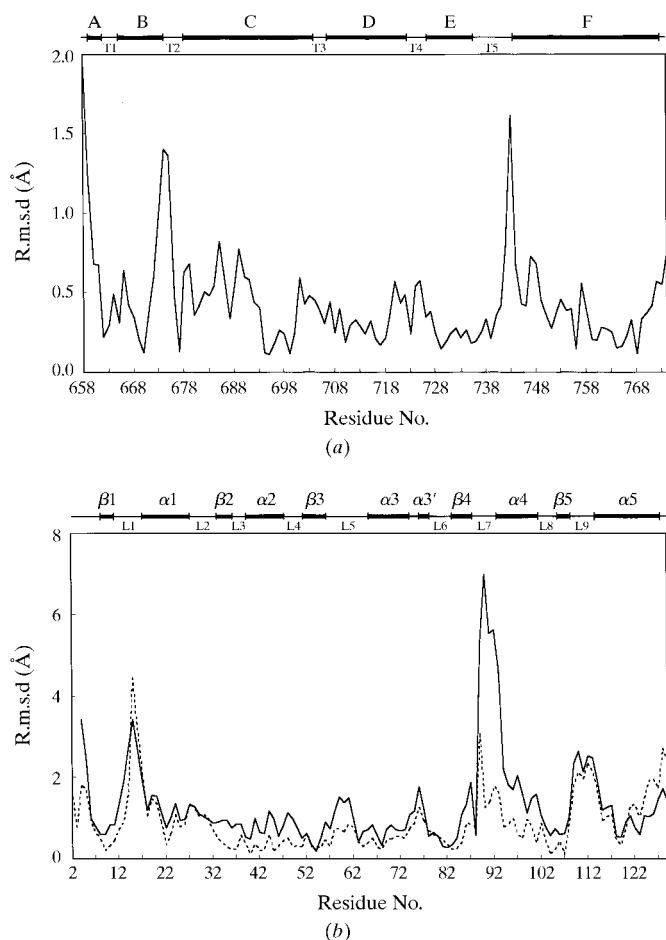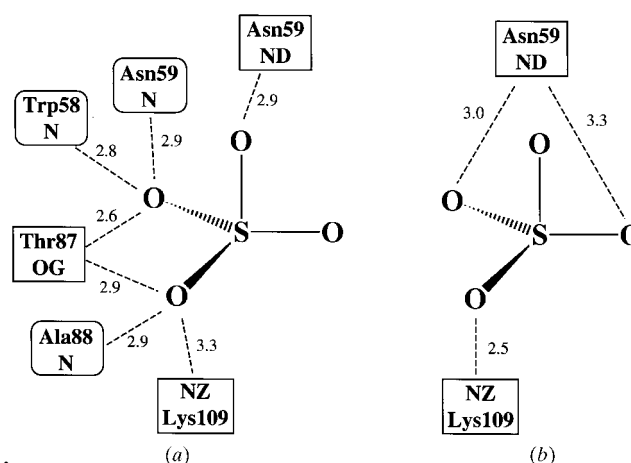

(*a*)

(*b*)

Figure 5
Plot of the r.m.s. deviations in C^α position. (*a*) The differences between the HPt domain complexed with CheY and the 2.06 Å HPt domain with the schematic secondary structure of the complexed HPt domain. (*b*) The differences between the complexed CheY and Mg^{2+}-CheY (solid line) and between the complexed CheY and apo-CheY (dashed line). The schematic secondary structure of the complexed CheY is included.

(*a*)   (*b*)

Figure 6
A graphic representation of the hydrogen bonds to SO_4^{2-} ions. (*a*) The SO_4^{2-} ion in the complex structure and (*b*) the SO_4^{2-} ion in the apo-CheY structure. Hydrogen bonds are shown as dashed lines with their distance in Å. The residues whose side chains participate in the hydrogen bonding are represented as rectangles and the residues whose main chains participate in the hydrogen bonding are represented as ovals.

C-terminus by one residue, in contrast to helix $\alpha4$, the first turn of which was unwound. According to mutational analyses, Tyr106 of CheY is thought to be a switch residue which changes the rotation of the flagellar motor (Ganguli *et al.*, 1995; Zhu *et al.*, 1996, 1997). The rearrangement of loop L7 enables the side chain of Tyr106 to form a hydrogen bond (2.7 Å) with the main chain of Glu89. This 'in' position of Tyr106 has been suggested to change the rotation of the flagellar motor (Zhu *et al.*, 1997).

Loop L9 shifted away from the active site by more than 2 Å. There is no distinct difference in this region between apo-CheY and Mg^{2+}-CheY. The succeeding helix $\alpha5$ was involved in contact regions #3 and #4 on both sides of the helix. The side chain of Glu117 of helix $\alpha5$ formed a hydrogen bond with Arg760 of the HPt domain (region #3), whereas the NZ atom of Lys119 formed a hydrogen bond with the main-chain O atom of Val675 on the opposite side (region #4). These hydrogen bonds produced a rotation of $\alpha5$ by about 5° around its centre as a pivot, accompanied by a shift of loop L9. Lys109 in this loop is almost fully conserved in all bacterial response regulators, preceding the *cis*-proline 110 (Volz, 1993). Although C_α of Lys109 also moved more than 1.7 Å, the side-chain NZ atom was located at almost the same position as other CheY structures and was bound to one of the carboxyl O atoms of Asp57 as well as apo-CheY. The conformation change of the χ_1 angle from *gauche$^-$* (apo-CheY, 69°; Mg^{2+}-CheY, 56°) to *gauche$^+$* ($-73°$) enabled this interaction of Lys109.

The SO_4^{2-} ions of the current CheY and apo-CheY were both located in the active pocket. In the complex structure, the side chain of Lys658 of the HPt domain was located over the active pocket of CheY and pushed the SO_4^{2-} ion into the active pocket, 3 Å from the corresponding position of the apo-CheY SO_4^{2-} ion. As a result, the SO_4^{2-} ion formed more hydrogen bonds than in apo-CheY (Figs. 1*c* and 6). Since the position of the S atom corresponded to a point only 2.0 Å from a carboxyl O atom of Asp57 of apo-CheY, the SO_4^{2-} ion appeared to be located at the site where a phosphoryl group might be placed when CheY is phosphorylated. To avoid the collision with the SO_4^{2-} ion, however, the side chain of Asp57 of CheY rotated toward the bottom of the active pocket and formed a hydrogen bond with the side chain of Asp12.

Since the active residue His715 of the HPt–CheY was not involved in any interaction with CheY, the complex structure does not represent the binding mode which caused the phosphotransfer reaction. ArcB contains both the HPt domain and a receiver domain, which is represented by CheY. One of the four interactions between the HPt domain and CheY shown in this structure might be an example of the interaction of these domains in the ArcB molecule. However, a detailed discussion must wait until we obtain the three-dimensional structure of the intact ArcB or at least of the receiver–HPt domain of ArcB.

References

Baikalov, I., Schröder, I., Kaczor-Grzeskowiak, M., Grzeskowiak, K., Gunsalus, R. P. & Dickerson, R. E. (1996). *Biochemistry*, **35**, 11053–11061.

Bellsolell, L., Prieto, J., Serrano, L. & Coll, M. (1994). *J. Mol. Biol.* **238**, 489–495.

Brünger, A. T. (1990). *Acta Cryst.* A**46**, 46–57.

Brünger, A. T. (1992). *X-PLOR Version* 3.1: *A System for X-ray Crystallography and NMR.* New Haven: Yale University Press.

Collaborative Computational Project, Number 4 (1994). *Acta Cryst.* D**50**, 760–763.

Cowtan, K. D. & Main, P. (1996). *Acta Cryst.* D**52**, 43–48.

Djordjevic, S., Goudreau, P. N., Xu, Q., Stock, A. M. & West, A. H. (1998). *Proc. Natl Acad. Sci. USA*, **95**, 1381–1386.

Ganguli, S., Wang, H., Matsumura, P. & Volz, K. (1995). *J. Biol. Chem.* **270**, 17386–17393.

Georgellis, D., Lynch, A. S. & Lin, E. C. C. (1997). *J. Bacteriol.* **179**, 5429–5435.

Higashi, T. (1989). *J. Appl. Cryst.* **22**, 9–18.

Hutchinson, E. G. & Thornton, J. M. (1996). *Protein Sci.* **5**, 212–220.

Ishige, K., Nagasawa, S., Tokishita, S. & Mizuno, T. (1994). *EMBO J.* **13**, 5195–5202.

Iuchi, S., Matsuda, Z., Fujiwara, T. & Lin, E. C. C. (1990). *Mol. Microbiol.* **4**, 715–727.

Jones, T. A., Zou, J.-Y., Cowan, S. W. & Kjeldgaard, M. (1991). *Acta Cryst.* A**47**, 110–119.

Kato, M., Ishige, K., Mizuno, T., Shimizu, T. & Hakoshima, T. (1996). *Acta Cryst.* D**52**, 1214–1215.

Kato, M., Mizuno, T. & Hakoshima, T. (1998). *Acta Cryst.* D**54**, 140–142.

Kato, M., Mizuno, T., Shimizu, T. & Hakoshima, T. (1997). *Cell*, **88**, 717–723.

Kraulis, P. J. (1991). *J. Appl. Cryst.* **24**, 946–950.

Laskowski, R. A., MacArthur, M. W., Moss, D. S. & Thornton, J. M. (1993). *J. Appl. Cryst.* **26**, 283–291.

Luzzati, P. V. (1952). *Acta Cryst.* **5**, 802–810.

Lynch, A. S. & Lin, E. C. C. (1996). *J. Bacteriol.* **178**, 6238–6249.

McEvoy, M. M., Hausrath, A. C., Randolph, G. B., Remington, S. J. & Dahlquist, F. W. (1998). *Proc. Natl Acad. Sci. USA*, **95**, 7333–7338.

Madhusudan, Zapf, J., Whiteley, J. M., Hoch, J. A., Xuong, N. H. & Varughese, K. I. (1996). *Structure*, **4**, 679–690.

Nagasawa, S., Tokishita, S., Aiba, H. & Mizuno, T. (1992). *Mol. Microbiol.* **6**, 799–807.

Navaza, J. (1994). *Acta Cryst.* A**50**, 157–163.

Ramachandran, G. N. & Sasisekharan, V. (1968). *Adv. Protein. Chem.* **23**, 283–438.

Stock, A. M., Martinez-Hackert, E., Rasmussen, B. F., West, A. H., Stock, W. J., Ringe, D. & Petsko, G. A. (1993). *Biochemistry*, **32**, 13375–13380.

Stock, A. M., Mottonen, J. M., Stock, J. B. & Schutt, C. E. (1989). *Nature (London)*, **337**, 745–749.

Tsuzuki, M., Ishige, K. & Mizuno, T. (1995). *Mol. Microbiol.* **18**, 953–962.

Urzhumtseva, L. M. & Urzhumtsev, A. G. (1997). *J. Appl. Cryst.* **30**, 402–410.

Volkman, B. F., Nohaile, M. J., Amy, N. K., Kustu, S. & Wemmer, D. E. (1995). *Biochemistry*, **34**, 1413–1424.

Volz, K. (1993). *Biochemistry*, **32**, 11741–11753.

Volz, K. & Matsumura, P. (1991). *J. Biol. Chem.* **266**, 15511–15519.

Yaku, H., Kato, M., Hakoshima, T., Tsuzuki, M. & Mizuno, T. (1997). *FEBS Lett.* **408**, 337–340.

Zhu, X., Amsler, C. D., Volz, K. & Matsumura, P. (1996). *J. Bacteriol.* **178**, 4208–4215.

Zhu, X., Rebello, J., Matsumura, P. & Volz, K. (1997). *J. Biol. Chem.* **272**, 5000–5006.